Structural Studies of Halogen Acid Doped Polyaniline and the Role of Water Hydration

M. J. Winokur*

Department of Physics, University of Wisconsin, Madison Wisconsin 53706

B. R. Mattes

Los Alamos National Laboratory, Los Alamos, New Mexico 87545

Received April 14, 1998; Revised Manuscript Received August 3, 1998

ABSTRACT: The structural ordering within crystalline polyaniline (PANI) powders as emeraldine (i.e., at 50% oxidation) in both its base (EB) and halogen acid doped salt (ES) forms has been studied using X-ray diffraction. PANI−ES powder precipitates, obtained immediately after synthesis, have significant crystalline fractions which nominally approximate the proposed pseudo-orthorhombic type I (ES-I) salt structure (Pouget, J. P.; et al. *Macromolecules* **1991**, 24, 779). Additional treatments, such as dedoping by immersion in NH_4OH solution and redoping by aqueous HF acid, lead to further changes in the structure with the appearance of additional crystalline phases. The role of water hydration in this structural evolution is also examined, and significant structural variations are found to occur with radically different time scales. Comparison of the data with structure factor calculations leads to new structural models that identify changes in the PANI chain packing and, in the case of HCl doping, correlate these with the known variations in the charge transport properties.

1. Introduction

Polyaniline (PANI) and its related derivatives comprise an extremely diverse family of conducting polymers in terms of both electronic properties and structural characteristics. The chemical formula most broadly describing the parent polymer is

$$([(C_6H_4 - NH - C_6H_4 - NH-)_{1-x}][(C_6H_4 - N{=}C_6H_4{=}N-)_x])_n$$

and by variation of the oxidation state[1,2] PANI can be converted from the fully oxidized ($x = 1$) pernigraniline to the half-oxidized ($x = 0.5$) emeraldine base (EB) to the fully reduced ($x = 0$) leucoemeraldine forms. PANI polymers can also be obtained in a highly conducting salt form, either during synthesis or after reaction of EB with an appropriate acid HX, to yield

$$[(C_6H_4 - NH - C_6H_4 - NH^+-)(X^-)]_n$$

by protonation of the imine nitrogens with a nominal maximum dopant concentration of $y = 0.5$ where $y = X^-/N$. The specific details are intimately related to sample synthesis, processing, and handling conditions, and there currently exists an extensive literature.[3−7]

Fully amorphous or other highly disordered PANI emeraldine salts (ES) exhibit modest conductivities and a quasi-one-dimensional electron transport behavior indicative of poor interchain coupling. More highly ordered systems can exhibit significantly enhanced conductivities and, in some instances, display a metallic-like state.[8]

Despite these strides in improved synthesis and processing, many mysteries remain concerning the specific molecular level structural attributes and how these structure/property relationships influence the overall polymer host behavior.

Even in the case of some of the most well-known forms of PANI, i.e., EB (at $x = 0.5$) or ES (after protonic acid doping of EB), there exist only a few quantitative descriptions of the molecular chain structure and interchain packing.[9−12] This deficiency can be partially attributed to the underlying molecular level interactions which give rise to this proclaimed diversity. Local variations in the extent of hydrogen bonding,[13−15] the relative proportion of amine/imine linkages,[16] the relative concentration of primary dopants, and the inclusion of secondary guest species (e.g., water, secondary dopants)[17,18] are all contributing factors which can lead to distinctive sample-to-sample variations.

The most extensive structural studies of crystalline PANI are reported by Pouget and co-workers,[9,19−23] and there is a clear distinction between PANI samples prepared from the base or salt forms. Precipitated HCl-doped ES powders typically contain a significant proportion of a crystalline phase referred to as ES type I (or ES-I) with a proposed pseudo-orthorhombic unit cell approximate as shown in Figure 1b and lattice parameters as listed in Table 1. Dedoping, by treatment of ES-I with a 1.0 M aqueous ammonia solution, gives the base form (or EB-I) and, in work of Pouget et al.,[9] leads to a fully amorphous phase. Redoping with aqueous HCl once again gives an ES-I sample. Solvent-cast EB films exhibit a local structure different from that of EB-I, and these are referred to as EB type II or EB-II. EB-II films may be fully amorphous or partially crystalline. Treatment of EB-II with aqueous HCl then leads to a second crystalline salt polymorph, ES-II (also shown in Figure 1). PANI−ES samples containing a wealth of other acid dopants are reported,[24−29] but highly detailed structural models are generally sparse.

Secondary guests (or dopants) further complicate matters. Many PANI salts are found to be highly hygroscopic, and this water uptake can be associated

* To whom correspondence should be addressed.

10.1021/ma980586y CCC: $15.00
Published on Web 10/24/1998

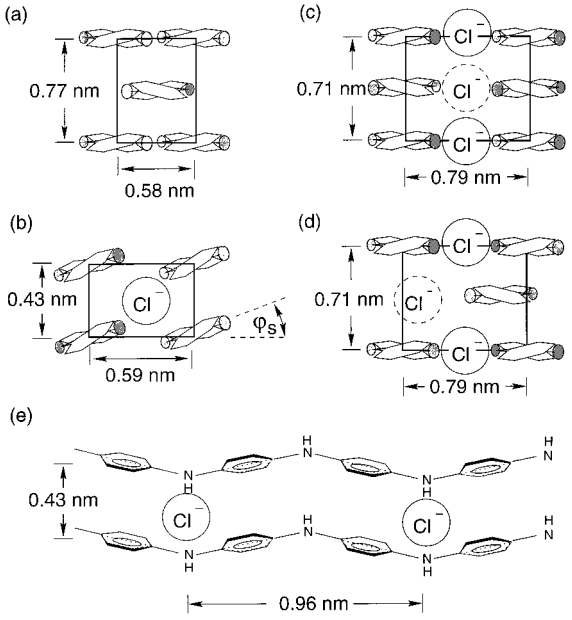

Figure 1. Proposed equatorial projections and lattice repeats for various PANI forms including (a) EB-II, (b) ES-I, (c) ES-II, P*c*2*a*, and (d) ES-II, $P2_122_1$. In addition, (e) contains a *c*-axis projection of ES-I showing the relative position and spacing of the Cl^- anion. (Adapted with permission from ref 9.)

with pronounced increases in the dc conductivities.[30,31] Although some of this enhancement may be associated with ion mobilities, in situ electron spin resonance (ESR) measurements[32] reveal a complex interplay between the localized electronic excitations, i.e., polarons and/or bipolarons, and this water uptake. These observations suggest that interdiffusion of water also initiates significant changes in the polymer microstructure. There are, at present, only a few scattering studies which have monitored PANI sample in response to changes in the moisture content.[17,33,34]

This paper contains results from X-ray scattering studies of HCl- and HF-doped ES-I PANI powders which further clarify the structural attributes within the class I family. Detailed comparisons to the proposed ES-I pseudo-orthorhombic approximate of Figure 1 and other related structural models demonstrate that, for both HCl- and HF-doped PANI−ES, this nominal model must be significantly modified. In the case of HF doping we observe two crystalline polymorphs (at $y \approx 0.25$ and $y \approx 0.50$), which are qualitatively different than that previously reported for HCl-doped ES-I samples. These basic studies are further extended by subsequent in situ investigations of various dried ES samples during continuous exposure to water vapor. In this latter process we observe pronounced, systematic changes in the scattering profiles both at the initial onset of water uptake and after longer time periods. Comparisons with possible candidate structures are also performed for samples saturated by water vapor. These modeling studies suggest that the inclusion of water molecules occurs along identifiable channels parallel to the polymer backbone and that hydration of HCl-doped PANI induces structural changes which enhance interchain packing.

2. Experimental Details

Materials. Aniline ($C_6H_5NH_2$, Mallinckrodt, St Louis, MO) was fractionally distilled in vacuo from barium oxide (5 mmHg, bp range 73−82 °C). Ammonium peroxydisulfate ($NH_4S_2O_8$) and 1-methyl-2-pyrrolidinone (NMP, $(CH_3)NC_4H_6O$), hydrochloric (HCl) and hydrofluoric (HF) acids (38%), and pyrrolidine (C_4H_9N) were used as purchased from Aldrich Chemical, Milwaukee, WI. Ammonium hydroxide, 29 wt % (NH_4OH, Mallinckrodt), was used as purchased. Tetrahydrofuran (THF) (C_4H_4O, Fischer Scientific, Fair Lawn, NJ) was dried with sodium benzophenone and vacuum distilled prior to use.

PANI powders were prepared by oxidative polymerization of aniline−HCl solutions according to the methods of ref 35. Typically, a 1 N HCl solution was prepared by addition of concentrated HCl to distilled deionized water. Then 1425 mL of this solution was placed into a 3000 mL polymerization vessel along with 122.7 g (1.32 mol) of aniline (maintained with stirring at 3 °C). A 1575 mL portion of 1 M HCl was combined with 69.03 g (0.303 mol) of ammonium peroxidisulfate in a separate flask. This mixture was stirred until the oxidant dissolved and then cooled to 0 °C. The persulfate solution was dropwise added to the aniline solution over the course of an hour. The combined solutions reacted for an additional 3.5 h. The green emeraldine HCl precipitate was collected, and then this powder was extracted first in water and then in methanol until the wash solutions were colorless. This as-synthesized HCl−ES was subsequently immersed in 5 L of 0.1 M NH_4OH for 3 h, filtered, and then washed once again with THF and methanol until the solutions were clear (yield, 24%). The purified EB was vacuum-dried ($<10^{-5}$ Torr) and stored in a vacuum desiccator. Four point probe dc conductivity measurements of a dried pressed EB-I powder after immersion in 4 M HCl for 24 h to form the fully doped ES-I was measured at 1.2 S/cm.

Individual EB-I portions were thereafter immersed in aqueous HF solutions ranging from 25 to 995 mM, then dried at 80 °C under dynamic vacuum for 24 h, and finally stored under dry N_2. These samples (including as-synthesized HCl−ES-I, dried HF−ES-I, and EB-I) were transferred in air into thin glass-, mica-, or beryllium-walled cells for diffraction studies. After a minimum 6 month exposure to ambient conditions, small quantities of the HCl-doped and representative HF-doped ES-I samples were transferred into X-ray glass capillaries, which were subsequently mounted into the sample side of a dual chambered, thermally controlled in situ vapor-doping cell. Diffraction profiles were acquired both before and after drying (ex situ at ca. 100 ° C for ~ 6 h). After the product was dried, a small quantity of degassed water was added to the second cell chamber. Powder diffraction profiles were then recorded at 15 or 30 min intervals after initiating exposure to water vapor for total times in excess of 24 h.

The X-ray data acquisition employed either one of two available diffractometers using a 15 kW rotating anode X-ray generator (Cu $\lambda_{K\alpha}$ Å). The first diffractometer employed a focusing bent graphite monochromator and a linear diode array (EG&G model XR1412) detector. The second diffractometer used an elastically bent LiF crystal and a 120° 2θ position sensitive detector (Inel model CPS-120). Both systems employed full He gas beam paths to minimize absorption and air scatter.

The modeling software was based on a custom-configured link-atom least-squares (LALS) Rietvelt refinement scheme.[36] Because of the limited number of distinguishable reflections and the presence of a significant amorphous scattering background, extended counting times (up to 12 h) were used to resolve weak or partially overlapping features. To reduce the effective parameter space of potential structures, the LALS algorithm included a second term, a Lennard-Jones (L-J) hard core packing repulsion ($\propto 1/r_{ij}^{12}$) for primary and secondary dopants only,[37] which constrained the nearest-neighbor distances of these nonbonded atoms. The actual form of the refinement residual was

$$R = x\frac{\sum_{2\theta}(I_{calc} - I_{expt})^2}{\sum_{2\theta}(I_{expt})^2} + (1 - x)\sum_{\text{unit cell}}^{r_{ij}<r_{cut-off}} \frac{a_{ij}}{r_{ij}^{12}}$$

Table 1. Calculated Unit Cell Parameters for Various Indicated Structural Phases

PANI sample	lattice repeats (Å)			angles (deg)			setting angle(s) ϕ_s (deg)	density (g/cm^3)
	a	*b*	*c*	α	*β*	*γ*		
HCl−ES-I (from ref 9)	5.9(**b**)	4.3(**a**)	9.6			90	20	
HCl−ES-I with H_2O	6.08	4.43	19.8	92	96	90	50	1.61
PANI EB-I	30	6.44	19.7	90	90	116	∼10	1.41
HF−ES-I*β* phase (dried)	6.03	7.57	19.2	86	90	88	25 40	1.51
HF−ES-I*β* with H_2O	5.82	7.77	19.4	85	85	84	25 60	1.63
HF−ES-I*γ* phase (dried)	6.53	9.14	19.0	82	90	87	20 50	1.23
HF−ES-I*γ* with H_2O	6.19	9.36	19.4	82	90	90	0 50	1.42
HCl−ES-I*γ* (dried)	5.89	8.73	19.7	90	81	90	5 50	1.43

where the relative contribution, *x*, and the L-J scaling coefficients, a_{ij}, and the r_{cutoff} were arbitrarily determined. Analogous procedures have proven helpful in studies of other polymeric hosts.[38] We note that while the specifics of the chosen background profiles and the various aforementioned fitting parameters are subjective, this procedure can rule out many potential, but unphysical, structural variants.

All modeling, of both EB and ES, used a four-monomer PANI chain repeat based on local structure studies of fully amorphous PANI.[11] A simpler two monomer construction, as used by Pouget and co-workers, would also be expected to fit the experimental data (the absence of *l* odd intensities notwithstanding). Small variations in the phenylene ring planarity or background profile also do not alter the main conclusions in the discussion that follows, although these attributes can slightly modify various model details (e.g., the chain setting angle or halogen ion position). Since PANI interchain packing interactions were also not considered by the modeling algorithm, the best-fit structures occasionally included a few unphysically close interchain pair spacings. Better knowledge of the local chain structure is necessary to address this shortcoming.

3. Experimental Results

3.1. Ex Situ Data and Modeling Analysis. Figure 2 sequentially displays representative X-ray profiles from the PANI powders studied, and there is always a superposition of amorphous and crystalline scattering. The as-precipitated HCl-doped ES-I profile (at bottom) qualitatively resembles those reported previously. The disparities in the peak widths and distinctive asymmetries suggest that some peaks result from multiple Bragg peak contributions. Dedoping, to yield EB-I, gave samples with significant crystallinity and profiles reminiscent of the HCl ES-I data but with clear shifts in both peak positions and intensities. One EB-I peak occurs at lower angle (near $2\theta = 7°$) and indicates a new, longer length scale *d* spacing. Treatment of this EB-I with aqueous HF acid solutions led to further changes in the scattering data and the appearance of two new sets of X-ray patterns neither of which resemble those of HCl−ES-I or the EB-I. These two structural phases are referred to, hereafter, as HF−ES-I*β* and HF−ES-I*γ* to distinguish them from the HCl−ES-I structure. The HF−ES-I*β* data suggests a modest reduction in the estimated crystallinity and the HF−ES-I*γ* structure, obtained only in samples exposed to 0.995 M HF solutions, is similar. Qualitatively this latter scattering pattern shows a strong resemblance to that of H_2SO_4-doped PANI powders.[24]

Comparisons of the powder data with profiles generated by structure factor calculations provide additional insight. Since previous HCl-doped PANI studies[9] only report a coexistence of undoped (or lightly doped) EB and the proposed pseudo-orthorhombic HCl−ES-I structure of Figure 1b, we assumed the presence of only a single, relatively homogeneous crystalline phase in combination with a background profile representing

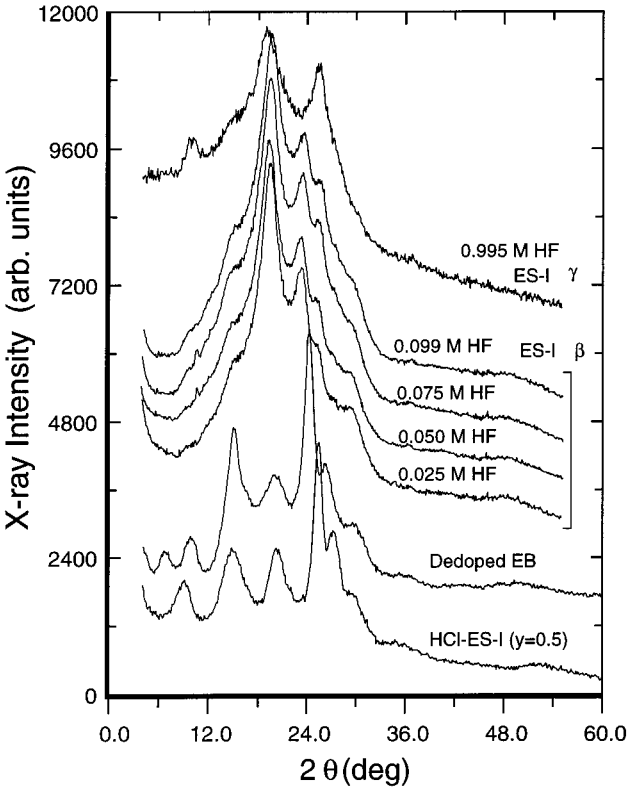

Figure 2. X-ray powder profiles from a series of emeraldine class I samples after synthesis (to yield HCl−ES at bottom), treatment with 0.1 M NH_4OH (to form EB-I), and then exposure to increasingly stronger aqueous HF solutions to give the *β* ($y \approx 0.25$) and *γ* ($y \approx 0.50$) forms of ES-I. Note: For clarity these curves have been vertically offset. (Adapted with permission from ref 34.)

scattering by the amorphous phase and parasitic contributions by the sample holder and "air". The bottom panel of Figure 3 compares the HCl−ES-I data ($y \approx 0.5$) to that obtained from a constrained variation of the orthorhombic ES-I structure of Pouget. In addition to the variations in the unit cell parameters and the PANI chain setting angle, ϕ_s, the two Cl^- ions in this unit cell were allowed to independently displace away from the channel center. While the calculated Bragg peak intensities are consistent with those reported by Pouget, direct comparison to the actual data is not satisfactory, especially for 2θ values spanning from 28° to 50°. While some improvement can be achieved by sharply increasing the background profile near $2\theta = 30°$, scattering by amorphous PANI (though of type II form) does not have this attribute and, thus, does not support this approach.

Significant deviations from this proposed model were therefore necessary. Since the sample had not been rigorously dried prior to the X-ray study, any realistic model required the presence of water. Thermgravimetric hydration studies of PANI suggest up to three water

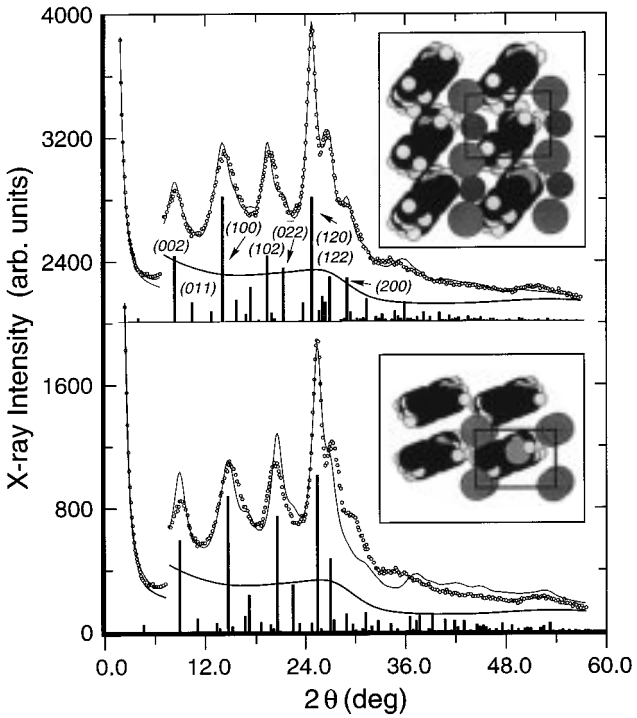

Figure 3. Bottom: Comparison of the calculated powder profiles (thin line) and experimental data (open dots) for an as-synthesized (i.e., containing water) HCl−ES-I sample using a model similar to the pseudo-orthorhombic model of ref 9. Top: Comparison of the calculated powder profile (thin line) and experimental data (open dots) for an as-synthesized (i.e., containing appreciable moisture) HCl−ES-I sample using a model which includes a second channel for absorbed water with $H_2O/Cl^- \equiv 2$. In addition these figures include the assumed background (includes contributions from amorphous PANI and residual "air" scatter) and the underlying Bragg reflections (as thick vertical bars).

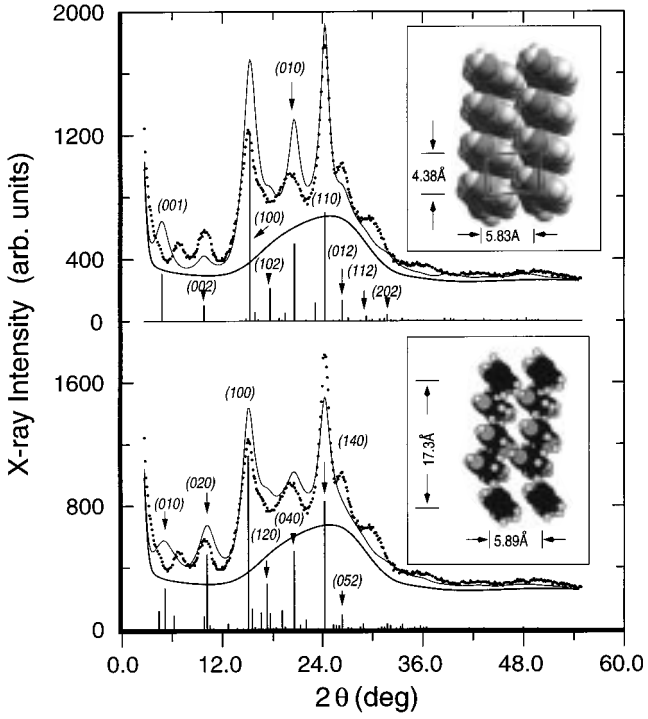

Figure 4. Bottom: Comparison of the calculated powder profiles (thin line) and experimental data (filled dots) for crystalline EB-I assuming a small unit cell similar to the pseudo-orthorhombic ES-I of ref 9 (or parts b and e of Figure 1). Top: Comparison of the calculated powder profiles (solid line) and experimental data (filled dots) for crystalline EB-I assuming a unit cell containing four PANI chains along the *b*-direction (17.3 Å). In addition these figures include an arbitrary background profile (thick line) and the underlying Bragg contributions (as thick vertical bars).

molecules per halogen ion are possible.[39] For the purposes of the structural refinement, a scaled oxygen "atom"[40] was assumed to coexist in, or near, the quasi-one-dimensional channels defined by linear arrays of the Cl^- ions with an approximate 2:1 water/chlorine ratio. Allowing for independent motion of water and Cl^- ion channels in combination with a lower unit cell symmetry (triclinic) resulted in major improvements in the refinements. Virtually all of the line shape asymmetries and anomalous broadening effects are satisfactorily reproduced by the linear superposition of the underlying Bragg peaks. A direct comparison is shown in the top panel of Figure 3 with unit cell parameters listed in Table 1, and for reference purposes, this structure is designated the ES α-phase. A notable attribute is the rather large setting angle, ϕ_s, of 50° vs 20° as proposed in ref 9. With respect to the average PANI molecular plane (to which ϕ_s is referenced), this gives nominal chain-to-chain spacings of 2.9 and 4.2 Å, respectively. Since a value of ~3.2 Å is the generally accepted minimum hard-core packing distance, the former spacing suggests that the actual setting angle is lower, although *significantly* larger than 20°. Another peculiar feature is that the (100) and (120) have nearly equal Bragg intensities but very different heights when viewed in the calculated profile. This difference arises from variations in their calculated widths. Thus the α-phase crystallites appear to be anisotropic in the equatorial plane with nominal coherence lengths of 40 and 60 Å, approximated from the Scherrer formula,[41] along the *a* and *b* directions, respectively. This is consistent with data from previously studies.[9,23] The distance from the Cl^- ion to the nearest PANI nitrogens ranges between 3.1 and 3.6 Å and is similar to that reported in amorphous HCl-doped PANI ES-II. Additionally there could be appreciable disorder within and between the two dopant channels. Further discussion relating this structure to enhancements in the electron transport is delayed until after the section reviewing the in situ hydration studies.

Dedoping of the α structure, in this work, led to a crystalline form of EB-I, as noted in the Introduction, which was not observed in the samples of ref 9. Well-ordered EB-I phases have been observed[42] elsewhere, although the underlying reasons for this behavior are not known. Since many of the crystalline EB-I features qualitatively resemble those of the HCl ES-I starting material, a prospective model based solely on α-phase chain packing was tried. A refined best-fit is shown in the top half of Figure 4. While there is some agreement with the experimental data in terms of peak positions, this small unit cell will never allow for a one-to-one peak identification in the lower angle region and, equally problematic, there are deviations in the relative peak intensities which cannot be addressed. Because of the pronounced scattering features at 2θ angles ranging from 2° to 6°, any new model required, at a minimum, a larger unit cell.

A recent article has postulated that the emeraldine four-unit phenylene ring repeat, BBQB (where B are Q are the bezenoid and quinoid forms, respectively), could provide for a nominal 4-fold increase in the unit cell size along the PANI EB-I [010] direction through a system-

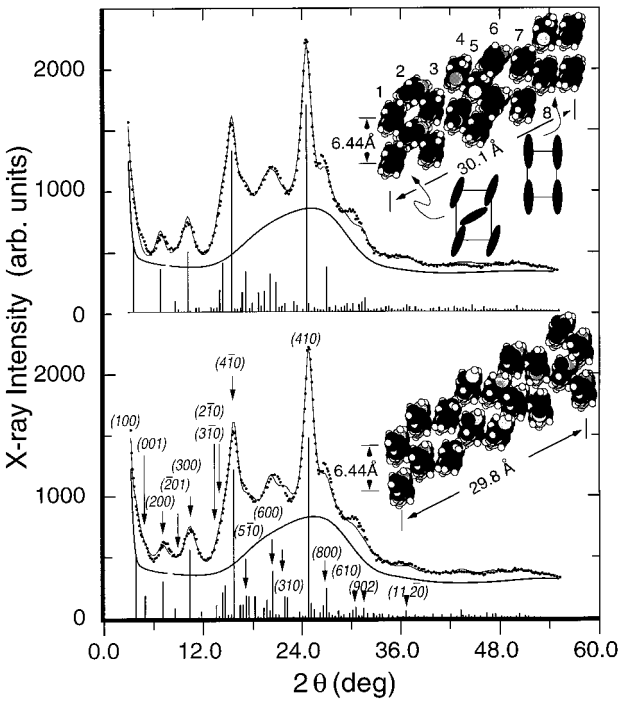

Figure 5. Two variations of the eight chain supercell used to reproduce the scattering profile of dedoped PANi-EB (type I). Bottom: Comparison of the calculated powder profiles (thin line) and experimental data (filled dots) for crystalline EB-I using an example that best reproduces the data at the lower 2θ angles. Top: This model best reproduces the data at the higher 2θ angles and exhibits local packing of the PANI chains which approximate both the ES-I and EB-II motifs. In addition these figures include an arbitrary background profile (thick line) and the underlying Bragg contributions (as thick vertical bars).

atic staggering of the chains along the chain axis.[43] As the bottom comparison of Figure 4 demonstrates, after introducing this larger unit cell and allowing for independent displacements of all four PANi chains, this still leads to poor agreement in the relative peak intensities and, at lower 2θ, peak positions.

Inspection of the low-angle 2θ scattering feature provides some evidence for a one-dimensional distortion having a 27 Å repeat. Since this spacing is inconsistent with the repeat along the chain axis or an integral number of repeats along the [100] or [010] directions, we assumed this *d*-spacing was within the equatorial plane and nominally along either the [110] or [1$\bar{1}$0] directions of the ES-I base model. Of these, an oblique 2D unit cell (of nominal dimensions 30 Å by 6.5 Å and $\gamma_{2D} = 116°$) containing *eight* PANi chains, as shown in Figure 5, satisfactorily reproduced all the features in the EB powder profile. All chains were allowed independent translations and, additionally, chain axis rotations. Although introduction of the 8-fold repeat is artificial, the fit is quite good and it may be viewed as indirect evidence for a supercell based on an integral number of repeats. Two example variations based on this large unit cell are shown in Figure 5 with the top one providing the best fit at higher 2θ angles and the bottom one at lower angles. A major feature of the schematic model, shown at top in Figure 5, is that it shows local chain packings reminiscent of both the ES-I structure and Pouget's proposed EB-II structure (see Figure 1a). Competing interactions which stabilize these two local structural motifs may, in part, be responsible for the presence of the large *d*-spacing.

In an alternate scenario one could postulate that this large *d*-spacing occurs along the polymer chain axis. This could be the situation if regularly spaced chain-folded lamellae were formed during processing as scanning tunneling microscopy[44] data has indicated in the preparation of type II samples. If so it seems rather surprising that this *d*-spacing is not clearly resolved in the ES samples spectra. As for the eight chain model above, the existence of relatively short crystallite coherence lengths is problematic. Clearly the possibility of other structural forms and/or the presence of multiple phases cannot be excluded.

All four HF−ES-Iβ data sets shown in Figure 2, as well as that of the HF−ES-Iγ sample, were acquired after rigorous drying under dynamic vacuum. The four HF−ES-I powder profiles representative of the proposed β phase show a number of systemic trends with increasing HF acid strength. The peaks centered at $2\theta = 20°$ and 26° intensify, while the peaks at $2\theta = 23°$ and 32° diminish. In addition there are a number of distinguishable features which form the low-angle shoulder in the region $10° \leq 2\theta \leq 18°$. These attributes did not significantly impact the modeling process. In all cases, there is no evidence for any residual EB-I because the relatively narrow and strong peak at $2\theta = 25°$ (for crystalline EB-I) is absent. However, prior to the X-ray scans, the samples were transferred in air. Moreover there are reports that a significant fraction of the absorbed water in PANI salts is so tightly bound that standard drying procedures do not extract all of the internal water.[33,45] For this reason the modeling of these samples included a small quantity of residual "water" fixed at one water molecule per two halogen anions by assuming a fractional occupancy at a number of related water sites. Modest changes in this concentration produced subtle variations in the specific internal details but did not alter the overall merit of a particular structural model.

Simple variations in the ES-I pseudo-orthorhombic base model did not yield acceptable fits to the HF−ES-Iβ or γ phase data. Since the HF−ES-Iβ phase represents an intermediate structure, a variety of larger unit cells incorporating a reduced number of anion channels were investigated. Of these the model structure providing the best overall fit to the experimental data (with $y \approx 0.25$) is shown in Figure 6 (at bottom) in combination with the as-indicated underlying Bragg peaks. This phase has an equatorial unit cell comprised of a single anion channel per two PANI chains each of which displays a different setting angle. All observed peaks and shoulders are extremely well reproduced although the fit itself would be better if the (0$\bar{2}$2) and (120) reflections had slightly different calculated intensities.

Since this proposed HF−ES-Iβ model represents an intermediate structure in the progression to the HF−ES-Iγ phase, further evolution requires (1) an increase the number of ion channels, (2) an increase the intra-channel density, or (3) a fundamental disruption of the β phase to yield a new structure. Recent studies of alkali-metal-doped PPV[46] have consistently identified that the first mechanism is the most prevalent response. A simple structure distortion which effects an increase in the relative number of channels is depicted in the top inset of Figure 6. In this scheme simple counter-propagating rotations of the two PANI chains (per projected 2D unit cell) are combined with a modest increase the *a* and *b* lattice repeats to form a larger

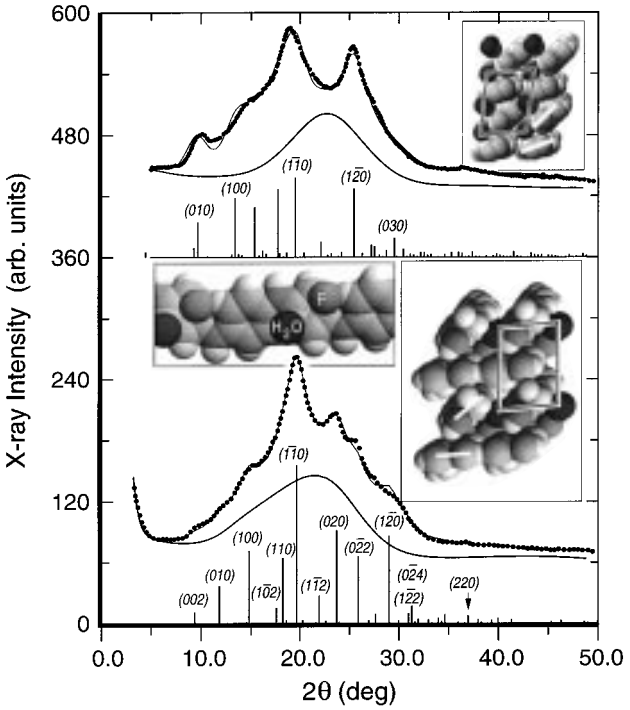

Figure 6. Bottom: Comparison of the calculated powder profiles (thin line) and experimental data (filled dots) for a dried HF−ES-Iβ phase sample using the model unit cell shown in the inset. Top: Comparison of the calculated powder profile (thin line) and experimental data (filled dots) for a dried HF−ES-Iγ phase sample using a model which includes a second quasi-one-dimensional chain of F^- ions to form a "dual" channel column. The specific unit cell parameters are given in Table 1. In addition these figures display the assumed background profile (thick line) and the underlying Bragg contributions (as thick vertical bars).

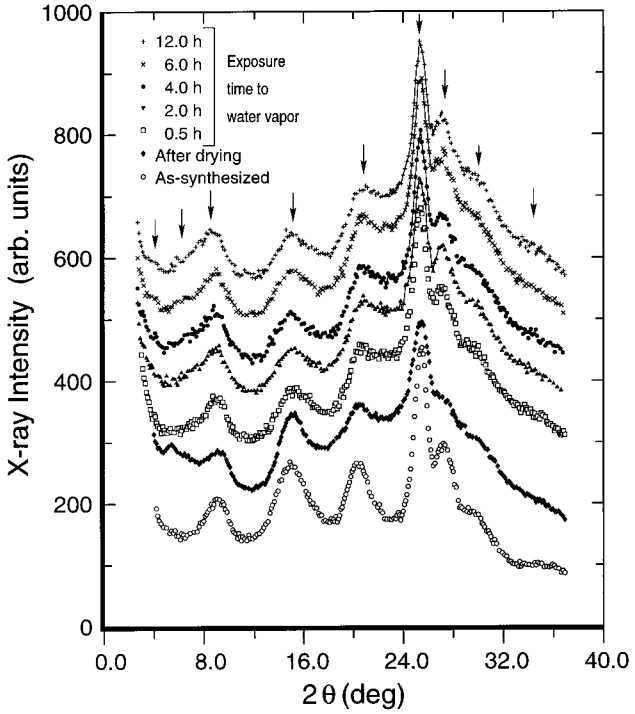

Figure 7. X-ray spectra recorded in situ from first the as-synthesized HCl−ES-I powder, then a dried powder, and, finally, during continuous exposure to water vapor. The curves are arranged so that six upper curves have been offset (for clarity) and the arrows are used to identify the major scattering features.

channel which then accommodates two parallel fluorine ion arrays while boosting the halogen concentration to $y \approx 0.5$. A slightly more uniform setting angle between the two PANI chains would tend to make the structure more closely resemble the nominal ES-I structure of Figure 1b.

Although the agreement is not as good as those of the previous modeled structures, it does reproduce much of the observed behavior. Moreover the formation of this "oversized" channel may facilitate the uptake of larger molecular dopant species such as sulfuric acid; hence the strong similarity of the HF−ES-Iγ data to that of H_2SO_4-doped PANI may be more than coincidental. Despite the lack of large numbers of well-defined Bragg peaks, the relatively simplistic approach by which all the observed data of the hydrated HCl-doped ES and the two dried forms of HF-doped ES can be addressed by intuitive variations in the original ES-I model of Pouget is an attractive scenario. These structural motifs also form the basis for the moisture absorption studies which now follow.

3.2. In Situ Studies of Emeraldine Salt Hydration and Modeling. The rapid uptake of moisture within rigorously dried HF- and HCl-doped ES powder samples, observed in situ, produced powder profiles with both overt and subtle variations. Figures 7 through 9 exhibit sequentially the changes in the X-ray scattering data before and after mounting in the in situ rehydration cell for the HCl ES-I powder, the β-phase HF−ES-I, and the γ-phase HF−ES-I samples, respectively. For the two HF-doped samples shown in Figures 8 and 9, which were stored over months in ambient conditions, the resulting changes due to slow moisture uptake are also quite pronounced, although there is near perfect recovery to the original powder line shape after rigorous drying.

All three samples demonstrated strong relative peak intensity variations in response to the removal of water. For instance, in Figure 8, the peaks located near 2θ values of 19°, 23°, and 25° have nearly the same height when the powders contain appreciable quantities of water, while the peak near 19° is significantly stronger than the other two after drying. In addition to the two or three most pronounced peaks, there are numerous weaker features which can be attributed to the presence of additional Bragg reflections. Most of these are indicated in the three figures by vertical arrows. In the ES-Iβ phase sample, the (110) and (1$\bar{1}$2) reflections tentatively identified in Figure 6 (near $2\theta = 18.5°$ and 21° respectively) become clearly distinguishable in many of the Figure 8 data sets. Analogous changes are seen in both Figures 7 and 9. In contrast the actual peak positions are relatively insensitive to variations in the moisture content implying that the unit cell dimensions remain relatively constant. Although water is considered to be a rather small molecule, this still suggests that there is considerable free volume within the intercalant channels, and this is consistent with the rather sparse average halogen anion repeat distance of approximately 9.5−10 Å along the PANI chain axis.

There are also pronounced intensity variations in the non-Bragg scattering contributions. Dried ES samples, especially the HCl-doped sample, always exhibited a very rapid intensity rise in the scattering intensity at 2θ angles below 4°. As Figure 10 demonstrates, this scattering feature became much less intense after the first 30 min of exposure to water vapor. A qualitatively

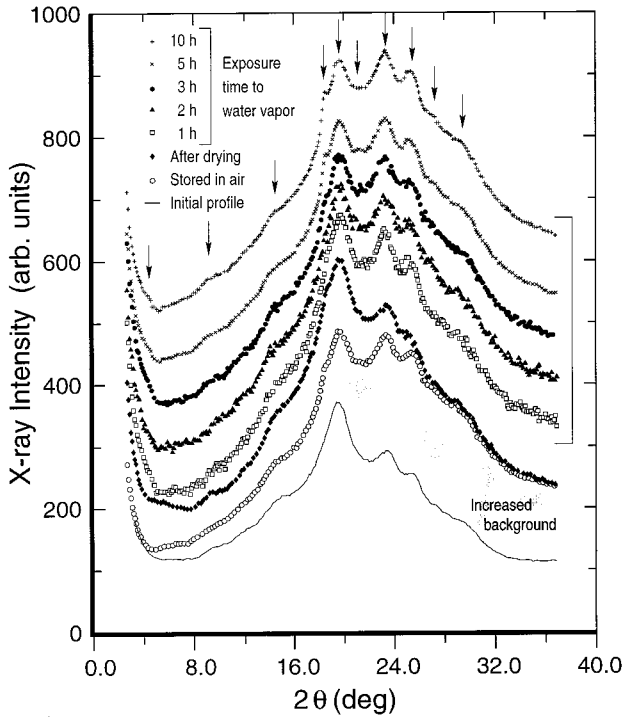

Figure 8. X-ray spectra recorded in situ from a dried HF−ES-Iβ phase powder (99.5 mM HF doped) as prepared, after storage at ambient conditions, dried again, and then during continuous exposure to water vapor. The curves are arranged so that the six uppermost curves have been offset (for clarity), and the arrows are used to identify the major scattering features. The shaded region is used to identify the 2θ region which shows an anomalous increase in the overall background due to water uptake.

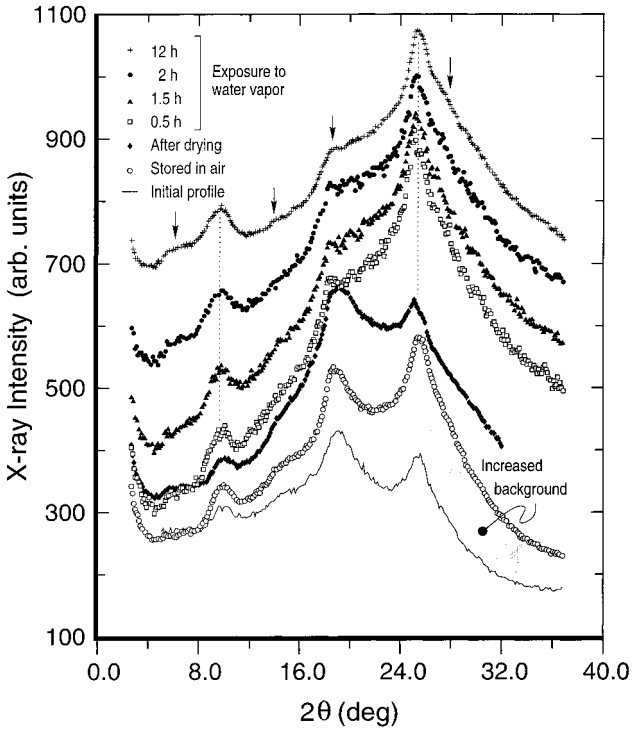

Figure 9. X-ray spectra recorded in situ from a dried HF−ES-Iγ phase powder (995 mM HF doped) as prepared, after storage at ambient conditions, dried again, and then during continuous exposure to water vapor. The curves are arranged so that the six uppermost curves have been offset (for clarity), and the arrows are used to identify the major scattering features. The shaded region is used to identify the 2θ region which shows an anomalous increase in the overall background due to water uptake.

similar response was observed in the HF-doped samples (not shown), although the variations were not nearly as prominent. This progression was also observed to have a component which extended to rather long times with noticeable changes still recorded even after 12 h of exposure. The wide-angle scattering features displayed only slight variations after the first hour. This suggests that the general packing features of the crystalline phases are quickly achieved while there is still a gradual evolution toward a state with a more homogeneous structural order.

Previous small-angle X-ray scattering (SAXS) studies[47] by Annis and co-workers (in type II materials) have observed a reduction in SAXS intensity along the meridional direction (i.e., parallel to the chain axis) when comparing EB and HCl-doped ES samples. If this is also true for these type I materials, then this non-Bragg attribute is most likely associated with the halogen anions and water molecules filling the channel. On this basis we postulate that changes in charge transport properties may result from two distinct mechanisms, a rapid variation due to evolution in the interchain packing and a much slower "annealing" response, more intrachain in character, arising from reorganization within the channels. Electron spin resonance (ESR) studies, which are sensitive to PANI chain charge excitations and exhibit a rather complex long-time behavior in PANI samples exposed to either moisture (or oxygen), are consistent with these observations.[32]

In contrast to the gradual falloff at the lower 2θ angles, there is a progressive increase in the overall background in the vicinity of 2θ angles near 32°. This

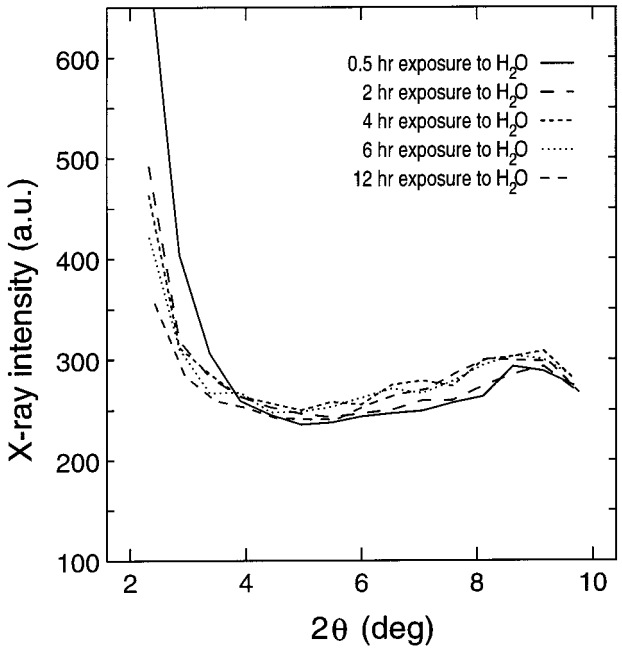

Figure 10. Low 2θ angle X-ray spectra recorded in situ from a dried HCl−ESI powder during continuous exposure to water vapor.

effect is most pronounced in the HF-doped ES samples and is identified by the shaded areas of Figures 8 and 9. The specific molecular level origin of this effect is unknown, but any significant water uptake would rapidly increase the number of pair distances in the range of 3 Å and, as such, could be expected to increase

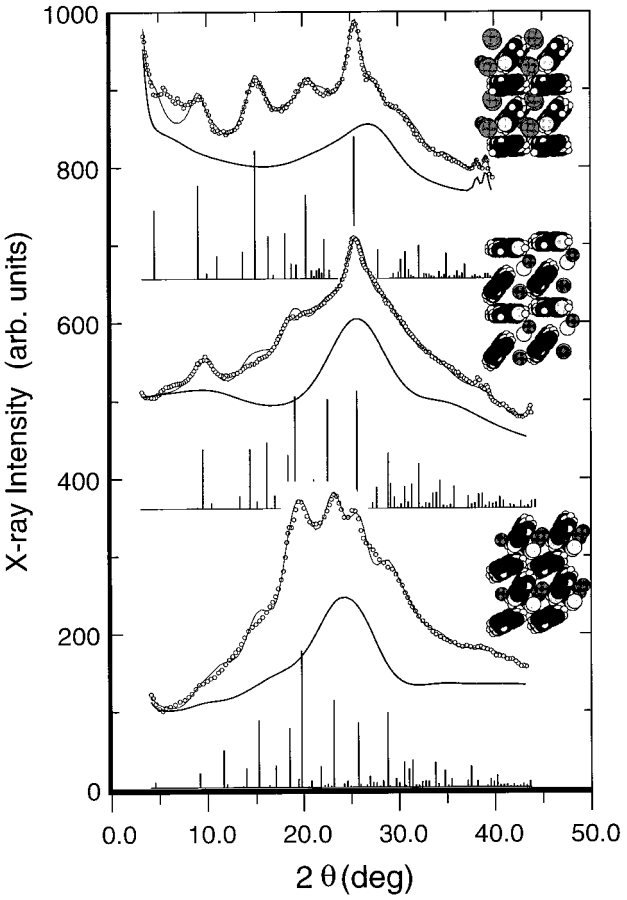

Figure 11. Comparison of the calculated powder profile (thin line) and experimental data (open circles) for (at top) dried HCl-doped ES-I powder and for (middle) HF-doped ES-Iγ phase and (bottom) HF-doped ES-Iβ phase powder samples after over 12 h of exposure to water vapor using the model shown in the respective insets. The specific unit cell parameters are given in Table 1. In addition each of these figures includes an arbitrary background profile (thick line) and the underlying Bragg contributions (as thick vertical bars).

the diffuse scattering contributions in this angular region, especially in the less dense amorphous fraction.

Structural modeling of the dried HCl−ES-I data using the nominal ES-I model of Figure 1b once again did not yield acceptable results (not shown). In this case a dual Cl-ion channel γ-phase structure is obtained after the "water-only" channels are removed, the unit cell is doubled along the *b*-direction, and two PANI chain setting angles are introduced. The topmost third of Figure 11 shows this structural modification in conjunction with the calculated and experimental profiles. Not only do the most intense Bragg scattering features have clearer one-to-one analogues in the scattering data but the necessary background profile is closer to that of Figure 3. Improvements in the fit in the vicinity of $2\theta = 6°$ would require implementation of an even larger unit cell and/or claims of additional structural phases. In direct comparison with the modified HCl-doped ES-Iα phase structure, as depicted at top in Figure 3, this γ-phase would be expected to exhibit noticeably poorer interchain charge transport properties because of the reduced π-orbital overlap between neighboring PANI chains. On the other hand, the moisture-laden α-phase structure has a stacking configuration known to enhance transport properties, although the lateral offset (parallel to the PANI major axis) between neighboring chains is quite significant. This latter observation may, in part, limit the evolution toward a highly conductive metallic-like state in the HCl-doped samples. In comparison H_2SO_4-doped poly(*p*-phenylenevinylene) can exhibit metallic-like behavior[48] with a similar structure having a chain-to-chain spacing close to 3.3 Å[49,50] and only a minimal "offset."

Modeling of the water-saturated HF-doped samples required only minor changes in the β- and γ-phase unit cell structures. In both cases the additional water is accommodated by increasing the water/fluorine ratio to 2:1 and letting these new constituents relax within the channels established by the fluorine anions. Unlike the α-phase structure seen in the as-synthesized HCl sample, in both studies HF−ES-I samples appear to retain the basic packing structure of the dried compound. Naively one may expect a smaller ion such as F^- to be less disruptive than Cl^- but since doping occurs in an aqueous media and fluorine is known to have a large solvation sphere, this is clearly not the case. Explicit comparisons to the experimental data are shown in the middle and bottom portions of Figure 11 using lattice parameters listed in Table 1. The overall quality of these model fits is somewhat worse than that for the dried powders but still *significantly* better than any simple variation of the nominal ES-I structure of Figure 1b. In most instances the failing is in the relative peak intensities and not in the actual peak positions. Increasing the moisture level beyond the arbitrary 2:1 ratio tended to further improve the agreement.

4. Discussion and Conclusions

There are a number of observations which require cross-correlating the many data sets and model parameters. In general the estimated peak widths of the constituent Bragg reflections are measurably broader in the dehydrated samples. A lower limit of approximately 30 Å for the nominal crystal coherence length is consistent with the full set of experimental data. Hence a proposed increase in the extent of the metallic islands during water uptake, as postulated by Kahol and co-workers from in situ ESR studies,[32] is supported by this X-ray study. Still this effect must be considered with respect to the entire range of the structural response, especially the wholesale changes in the unit cell structure during rehydration.

Of the three salts studied during moisture uptake, only the as-synthesized HCl-doped PANI showed significant irreversibility and then only with respect to the initial drying process. Direct comparisons of the dried HCl−ES-I powder profile in Figure 7 with that of Figure 3 in ref 9 (at $y \approx 0.5$) is difficult because the data that most resembles the previously published data are the profiles obtained after exposure to moisture. We suggest that the previous samples were either incompletely dried or inadvertently exposed to water during their handling. Hence the pseudo-orthorhombic ES-I template structure ("α"-phase) as previously proposed is qualitatively correct but underestimates the PANI chain setting angle and situates the Cl^- anions in the wrong channel position. On the other hand, our results for dried HCl-doped PANI salts suggest that similarly treated samples actually adopt a γ-phase packing motif.

The structure modeling consistently identifies the location of the Cl^- anion, in the direction parallel to PANi chain axis, at or near the position of the amine nitrogens whether or not water has been absorbed into

the matrix. The results from HF doping are similar but, since water and fluorine have nearly equivalent X-ray scattering strengths, it is impossible to verify the possibility of substitutional disorder by displacement of the fluorine by water molecules. There are also limitation in the cited unit cell parameters. The variations in the calculated chain or *c*-axis repeats (seen in Table 1) are not especially significant and, without oriented samples and/or dramatically improved crystallinity, little more can be deduced.

From inspection of the other unit cell parameters there are a number of trends which can be distinguished. Those equatorial packings characterized by one halogen anion array per PANI chain (α or γ phase) have significantly larger equatorial unit cell repeats than samples with a PANI chain:halogen anion column ratio of 2:1. Moisture uptake does alter the **a** and **b** repeats, but the overall change in the equatorial area per chain is rather minimal. Any "in situ" solvation of the halogen anions resulting from the extensive moisture uptake is constrained by the channel geometry.

The primarily goal of this study has been to rigorously test the validity of the original ES-I model proposed almost 7 years ago.[9] Under the assumption of a single relatively homogeneous single-doped phase model, we find that, while the original model structure has merit, the experimental data support a scenario in which there is a far more complex family of related structures. Not only do these new structural phases provide a better fit to the existing data but they also consistently identify the structural attributes which enhance the conductivity upon water uptake in HCl-doped PANI. It still remains to be seen how applicable these new phases are in the zoo of emeraldine salts now available although, in the largest molecular dopants, there is clearly a crossover from a channel motif to a lamellar packing.[12,27,28]

Acknowledgment. We gratefully acknowledge the support of this work through NSF Grant DMR-9631575 (M.J.W.) and by the DOE AIM Program (B.R.M.).

References and Notes

(1) MacDiarmid, A. G.; Chiang, J. C.; Halpern, M.; Huang, W. S.; Mu, S. L.; Somasiri, N. L. D.; Wu, W.; Yaniger, S. I. *Mol. Cryst. Liq. Cryst.* **1985**, *121*, 173.
(2) Huang, W. S.; Humphrey, B. D.; MacDiarmid, A. G. *J. Chem. Soc., Faraday Trans.* **1986**, *82*, 2385.
(3) Genies, E. M.; Boyle, A.; Laplowsi, M.; Tsintavis, C. *Synth. Met.* **1990**, *36*, 139.
(4) Cao, Y.; Smith, P.; Heeger, A. J. *Synth. Met.* **1992**, *48*, 91.
(5) Heeger, A. J.; Smith, P. In *Conjugated Conducting Polymers*; Keiss, H. G., Ed.; Springer-Verlag: New York, 1992; Vol. 102, p 141.
(6) Andreatta, A.; Tokito, S.; Moulton, J.; Smith, P.; Heeger, A. J. In *Science and Applications of Conducting Polymers*; Salaneck, W. R., Clark, D. T., Samuelsen, E. J., Eds.; Adam Hilger: Bristol, 1991; p 105.
(7) Gregory, R. In *Handbook of Conducting Polymers*, 2nd ed.; Skotheim, T., Elesenbaumer, R., Reynolds, J., Eds.; Marcel-Dekker: New York, 1998; Chapter 18, p 437.
(8) Menon, R.; Yoon, C.; Moses, D.; Heeger, A. In *Handbook of Conducting Polymers*, 2nd ed.; Skotheim, T., Elesenbaumer, R., Reynolds, J., Eds.; Marcel-Dekker: New York, 1998; Chapter 2, p 27.
(9) Pouget, J. P.; Jòzefowicz, M. E.; Epstein, A. J.; Tang, X.; MacDiarmid, A. G. *Macromolecules* **1991**, *24*, 779.
(10) Baughman, R. H.; Wolf, J. F.; Eckhardt, H.; Shacklette, L. W. *Synth. Met.* **1988**, *25*, 121.
(11) Winokur, M. J.; Mattes, B. R. *Phys. Rev. B* **1996**, *53*, R463.
(12) Luzny, W.; Samuelsen, E.; Djurado, D.; Nicoulau, Y. *Synth. Met.* **1997**, *90* (1), 19.
(13) Colomban, P.; Gruger, A.; Novak, A.; Régis, A. *J. Mol. Sci.* **1994**, *317*, 261.
(14) Gruger, A.; Colomban, P.; Novak, A.; Régis, A. *J. Mol. Sci.* **1994**, *328*, 153.
(15) Zheng, W.; Angelopoulos, M.; Epstein, A.; MacDiarmid, A. *Macromolecules* **1997**, *30*, 2953.
(16) Ray, A.; Richter, A. F.; MacDiarmid, A. G.; Epstein, A. J. *Synth. Met.* **1989**, *29*, E151.
(17) Lubentsov, B.; Timofeeva, O.; Saratovskikh, S.; Krinichnyi, V.; Pelkh, A.; Dmitrenko, V.; Khidelkel, M. *Synth. Met.* **1992**, *47*, 187.
(18) MacDiarmid, A. G.; Epstein, A. J. *Synth. Met.* **1995**, *69*, 85.
(19) Jòzefowicz, M. E.; Laversanne, R.; Javadi, H. H. S.; Epstein, A. J.; Pouget, J. P.; Tang, X.; MacDiarmid, A. G. *Phys. Rev. B* **1989**, *39*, 12958.
(20) Pouget, J. P.; Jòzefowicz, M. E.; Epstein, A. J.; Masters, J. G.; Ray, A.; MacDiarmid, A. G. *Macromolecules* **1991**, *24*, 5863.
(21) Laridjani, M.; Pouget, J. P.; Scherr, E. M.; MacDiarmid, A. G.; Jòzefowicz, M.; Epstein, A. J. *Synth. Met.* **1992**, *51*, 95.
(22) Pouget, J. P.; Laridjani, M.; Jòzefowicz, M. E.; Epstein, A. J.; Scherr, E. M.; MacDiarmid, A. G. In *Materials Research Society Symposium Proceedings;* Materials Research Society: Washington, DC, 1992; Vol. 247, p 589.
(23) Epstein, A. J.; Joo, J.; Kohlman, R. S.; Du, G.; MacDiarmid, A. G.; Oh, E. J.; Min, Y.; Tsukamoto, J.; Kaneko, H.; Pouget, J. P. *Synth. Met.* **1994**, *65*, 149.
(24) Moon, Y. B.; Cao, Y.; Smith, P.; Heeger, A. J. *Polymer* **1989**, *30*, 196.
(25) Yang, C. Y.; Smith, P.; Heeger, A. J.; Cao, Y.; Osterholm, J. *Polymer* **1994**, *35*, 1143.
(26) Lux, F.; Samuelsen, E. J.; Kang, E. *Synth. Met.* **1995**, *69*, 167.
(27) Minto, C.; Vaughan, A. *Polymer* **1997**, *38*, 2683.
(28) Song, H.; Park, D.; Lee, C.; Rhee, S.; Wang, X. *Mol. Crys. Liq. Cryst.* **1997**, *38*, 2683.
(29) Kim, J.; Kim, J.; Sung, H.; Kim, H.; Yoon, C.; Lee, H. *Synth. Met.* **1996**, *84*, 71.
(30) Pinto, N.; Shah, P.; Kahol, P.; McCormick, B. *Phys. Rev. B* **1996**, *53*, 10690.
(31) Price, W.; Wallace, G. *Polymer* **1996**, *37*, 917.
(32) Kahol, P.; Dyakonov, A.; McCormick, B. *Synth. Met.* **1997**, *89*, 1997.
(33) Boyle, A.; Penneau, J.; Genies, E.; Riekel, C. *J. Polym. Sci., Polym. Phys.* **1992**, *30*, 265.
(34) Winokur, M.; Mattes, B. *J. Plas. Rein. Comput.*, in press.
(35) Maron, J.; Winokur, M. J.; Mattes, B. R. *Macromolecules* **1995**, *28*, 4475.
(36) Prosa, T. Ph.D. Thesis, University of Wisconsin, 1996.
(37) PANI chain-to-chain interactions were not considered.
(38) Nishimura, H.; Sarko, A. *Macromolecules* **1991**, *24*, 771.
(39) Matveeva, E.; Calleja, R. D.; Parkhutik, V. *Synth. Met.* **1995**, *72*, 105.
(40) To first order the "atomic" form factor of an oxygen atom and a water molecule differ by two electrons.
(41) Alexander, L. E. *X-ray Diffraction Methods in Polymer Science*; Wiley-Interscience: New York, 1969.
(42) Colomban, P.; Gruger, A.; Régis, A.; Michael, D. *J. Chim. Phys.* **1995**, *92*, 954.
(43) Pouget, J. P.; Epstein, A. J. *Synth. Met.* **1994**, *65*, 139.
(44) Ho, P.; Zhang, P.-C.; Zhou, L.; Li, S.; Chan, H. *Phys. Rev. B* **1997**, *56*, 15919.
(45) Kahol, P. Private communication.
(46) Mao, G.; Winokur, M. J.; Karasz, F. E. *Phys. Rev. B* **1996**, *53*, R463.
(47) Annis, B. K.; Lin, J. S.; Scherr, E. M.; MacDiarmid, A. G. *Macromolecules* **1989**, *25*, 429.
(48) Ahlskog, M.; Menon, R.; Heeger, A.; Noguchi, T.; Ohnishi, T. *Phys. Rev. B* **1997**, *55*, 6777.
(49) Masse, M. A.; Schlenoff, J. B.; Karasz, F. E.; Thomas, E. L. *J. Polym. Sci., Polym. Phys. Ed.* **1989**, *27*, 2045.
(50) Mao, G.; Winokur, M. J.; Karasz, F. E. *Phys. Rev. B* **1998**, *58*, 4089.

MA980586Y